Journal of Power Sources 266 (2014) 162–169

Contents lists available at ScienceDirect

Journal of Power Sources

journal homepage: www.elsevier.com/locate/jpowsour

Identification of a new pseudo-binary hydroxide during calendar corrosion of (La, Mg)$_2$Ni$_7$-type hydrogen storage alloys for Nickel–Metal Hydride batteries

J. Monnier [a,*], H. Chen [a], S. Joiret [b,c], J. Bourgon [a], M. Latroche [a]

[a] ICMPE, UMR 7182 CNRS UPEC, 2-8 rue Henri Dunant, 94320 Thiais, France
[b] Sorbonne Universités, UPMC Univ. Paris 06, UMR 8235, Laboratoire Interfaces et Systèmes Electrochimiques, F-75005 Paris, France
[c] CNRS, UMR 8235, LISE, F-75005 Paris, France

HIGHLIGHTS

- The calendar corrosion of Ni–MH battery alloy system (La, Mg)$_2$Ni$_7$ is investigated.
- Combination of μRaman and TEM allows full characterisation of corrosion products.
- Influence of Mg substitution in the binary La$_2$Ni$_7$ on corrosion is demonstrated.
- La corrodes as La(OH)$_3$ needles with inner hollow nanochannels.
- The formation of a pseudo-binary hydroxide Mg$_{1-x}$Ni$_x$(OH)$_2$ is evidenced.

GRAPHICAL ABSTRACT

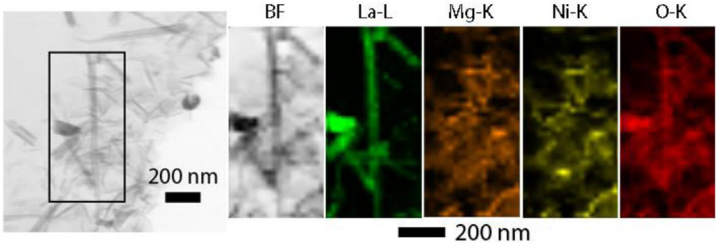

EDX-STEM mapping on La$_{1.5}$Mg$_{0.5}$Ni$_7$ sample corroded 8 weeks: correlation of Mg and Ni distribution

ARTICLE INFO

Article history:
Received 27 February 2014
Received in revised form
24 April 2014
Accepted 3 May 2014
Available online 13 May 2014

Keywords:
Corrosion
Ni–MH batteries
Raman micro spectroscopy
TEM
Combination of techniques

ABSTRACT

To improve the performances of Nickel–Metal Hydride batteries, an important step is the understanding of the corrosion processes that take place in the electrode material. In particular, the present study focuses for the first time on the model (La, Mg)$_2$Ni$_7$ system. The calendar corrosion in 8.7 M KOH medium was investigated from 6 h to 16 weeks immersion. By a unique combination of structural and elemental characterisations, the corrosion products are evidenced in those systems. In particular, we demonstrate that Ni and Mg combine in a pseudo-binary hydroxide Mg$_{1-x}$Ni$_x$(OH)$_2$ whereas La corrodes into nanoporous La(OH)$_3$ needles with inner hollow nanochannels.

1. Introduction

Because of their high capacity and the use of more environmentally friendly materials, Nickel–Metal Hydride (Ni–MH) batteries are expected to play a key role in the huge market of hybrid electric vehicles (HEV) and Emergency Light Units (ELU). Hydrogen-absorbing alloys based on ANi_5 (A: a rare earth such as La or a mixture of rare earths such as mischmetal Mm), or AB_5 when Ni is partially substituted by Mn, Co or Al, are widely used as negative electrode materials [1]. Recently, new families of hydrogen-absorbing alloys based on ANi_x, with $3 \leq x < 5$, have shown high interest because they

* Corresponding author.
E-mail address: monnier@icmpe.cnrs.fr (J. Monnier).

http://dx.doi.org/10.1016/j.jpowsour.2014.05.008
0378-7753/

present higher capacities than AB_5 alloys [2]. Moreover, some authors point out the beneficial substitution of the *A* element with lighter ones such as Mg, in these AB_x alloys [3]. In these systems, many studies focused on commercial compositions from the $PuNi_3$-type alloys. These AB_3 alloys present higher hydrogen storage capacity and higher discharge capacity, e.g. 356mAh/g for $LaCaMgNi_9$ [4] compared to the AB_5 alloys. Discharge capacity of 410mAh/g has even been achieved for the $La_{0.7}Mg_{0.3}Ni_{2.8}Co_{0.5}$ composition [5]. However the poor cycling stability of these new alloys prevent them from long cycle life practical application.

The life-time duration of these materials has to be significantly improved. When a hydrogen-absorbing alloy is used as negative electrode for an alkaline battery, the constituent elements are corroded by the electrolyte. This corrosion leads to loss of capacity balance between the positive and the negative electrode, loss of water and drying of the battery, and eventually to shortcut. Therefore, a good understanding of the corrosion processes will allow to find solutions to overcome these phenomena, and to finally improve the battery cycle life.

The degradation processes of AB_5-based Ni–MH batteries have been extensively studied during calendar storage and cycling [6–8]. In these alloys containing Mm, Ni and Co, the degradation process is closely related to alloy corrosion in aqueous KOH electrolyte and is enhanced by decrepitation (fracture of the powder particles creating new surfaces). The latter phenomenon is a consequence of volume changes occurring upon hydrogen solid solution/hydride phase transformation during cycling [9]. It has been observed that during soaking of AB_5 alloy into KOH aqueous solution, a continuous nanocrystalline corrosion scale composed of a metallic solid solution (Ni, Co), oxide solid solution (Ni, Co)O and mischmetal hydroxide $Mm(OH)_3$ needles form as surface corrosion products.

The AB_3 alloys previously mentioned [4] have also been studied regarding their high corrosion rates [10]. However, all these studies are limited to cycling degradation studies.

Concerning A_2B_7 alloys, few works have been published on commercial composition during electrochemical cycling [11]. The commercialized A_2B_7 moved from pure La-based $(La, Mg)_2Ni_7$ towards light rare earth rich mischmetal-based $(Mm, Mg)_2Ni_7$ to reduce the capacity degradation through cycling [12]. As an example, the studied composition $La_{0.7}Mg_{0.3}Ni_{3.4}Mn_{0.1}$ presents an initial capacity of 400 mAh/g which decreases continuously with cycling (down to 200 mAh/g for 35 cycles). The corrosion study identifies formation of a $Mg(OH)_2$ film then the formation of $La(OH)_3$ needles. However, neither the Ni nor the Mn corrosion products are mentioned. Considering the existing literature, a fundamental study to understand the corrosion process in A_2B_7 alloys is missing. Moreover, the peculiar role of Mg is not fully understood, and comparison between corrosion of binary and pseudo-binary compounds is necessary. This study aims to present a full characterisation of the corrosion processes taking place during the soaking of $(La, Mg)_2Ni_7$ alloys in alkaline medium (KOH).

2. Experimental part

2.1. Preparation of the alloys

The binary La_2Ni_7 alloy was prepared by induction melting of the pure elements (La, Ni: 99.9%) under vacuum in a water cooled copper crucible. The alloy was turned over five times to ensure good homogeneity and was annealed for seven days at 1000 °C. The pseudo-binary alloy $La_{1.5}Mg_{0.5}Ni_7$ was prepared in two steps by powder metallurgy. A precursor $LaNi_{4.67}$ was first prepared by induction melting as for the binary compound. This precursor was then grounded and mixed with Mg powder (99.8%). The mixture was annealed for ten days at 900 °C in a tight crucible closed under argon.

2.2. Calendar corrosion exposure

1.5 g of each alloy were exposed to 8.7 M KOH solution with the following conditions: immersion time between 6 h and 16 weeks; ambient temperature, argon desaerated atmosphere; daily homogenization to avoid preferential corrosion of part of the sample; constant ratio $m_{alloy}/V_{electrolyte}$; sampling of ~200 mg of powder for each immersion time. KOH 8.7 M was selected to emphasize the corrosion effect, without being detrimental to the specific conductivity of the solution [13].

Powder particles were rinsed down to a pH close to 12 (for pH < 12 the corroded species start to dissolve in water), then dried under vacuum at 40 °C for 24 h.

2.3. Characterisation techniques

Both initial alloys were characterised by microprobe analysis (EPMA) and X-ray diffraction (XRD). Corrosion products of A_2B_7 alloys powders were examined by XRD, Raman micro-spectroscopy (micro-RS), scanning electron microscopy (SEM) and transmission electron microscopy (TEM). A Bruker Da Vinci (Cu K_α radiation) and a Bruker D8 (Cu K_α radiation) were used for XRD analysis. Patterns were typically acquired with the Da Vinci between 10 and 110° (2θ) in 0.015° steps for 3 s, leading to an acquisition time of 5 h 30 min. Longer acquisition time (24 h) was performed for some samples with the D8 diffractometer for the same angular region.

Micro-RS measurements were performed using Notch filter based micro-spectrometer equipped with Peltier cooled CCD (Horiba Jobin Yvon) with a focal length of 180 mm, a 1800 lines/mm grating and an air cooled Ar^+ Laser emitting at 514.5 nm or HeNe Laser emitting at 632.8 nm. Spectral resolution is around 3 cm^{-1} and calibration is checked on the 520.5 cm^{-1} band of silicon. Microanalysis is achieved through Olympus microscope and 100× and 50× Olympus objective. The beam size is about 2 μm for a 100× and about 5 μm for a 50× objective. A laser excitation power of 70 μW is used. Spectra acquisitions are managed by the LabSpec software (Horiba Jobin Yvon).

Powder particles were examined with a Zeiss LEO scanning electron microscope equipped with a Field Emission Gun and an energy dispersive X-ray detector (EDX). No coating was made in order to be sure that the morphological changes observed at the alloy surface are due to the corrosion process.

A Tecnai FEI F20 ST equipped with EDX detectors provided high spatial resolution imaging of the scale morphology, crystallography (by electron diffraction) and chemistry (by EDX analyses) of the corrosion products. TEM specimens were prepared by cutting thin slices (60–80 nm) of resin embedded powder particles in an ultramicrotome.

3. Results

3.1. Pristine alloy characterisations

XRD pattern of the binary La_2Ni_7 compound was indexed in the Ce_2Ni_7 hexagonal cell ($P6_3/mmc$ space group). Pseudo-binary $La_{1.5}Mg_{0.5}Ni_7$ was observed under two polymorphic forms: Ce_2Ni_7 hexagonal ($P6_3/mmc$ space group) and Gd_2Co_7 rhombohedral (R-$3m$ space group). Results of the characterisation of both samples are given in Table 1.

3.2. Structural characterisation of corrosion products

Figs. 1a and 2a show the XRD patterns recorded for La_2Ni_7 and $La_{1.5}Mg_{0.5}Ni_7$, respectively, after immersion in 8.7 M KOH for different soaking times. Beside the alloy main diffraction peaks,

Table 1
Characterisation of the alloys by EPMA and XRD analysis.

Electron probe microanalysis (±0.01)	B/A ratio	Space group	%	Cell parameters		Volume V (Å^3)
				a (Å)	c (Å)	
La_2Ni_7	3.505 ± 0.117	$P6_3/mmc$	100	5.06284 (0.00004)	24.69757 (0.00028)	548.243 (0.009)
$La_{1.5}Mg_{0.5}Ni_7$	3.337 ± 0.122	$P6_3/mmc$	22.1 (0.5)	5.03144 (0.00010)	24.17544 (0.00097)	530.017 (0.026)
		R-3m	78 (1)	5.03124 (0.00009)	36.25952 (0.00093)	794.883 (0.028)

these diffractograms enable to identify the presence of the $La(OH)_3$ phase, especially at longer soaking times (additional X-ray diagrams are available in the Supplementary Information Fig. S1).

For a better phase identification, longer acquisition time (up to 24 h) allowing better signal to noise ratio was performed for both samples. $Ni(OH)_2$ for the binary alloy, and $Mg(OH)_2$ for the pseudo-binary one are clearly observed after 8 weeks of soaking (Figs. 1b and 2b).

Reference Raman spectra of O–H vibration of $Ni(OH)_2$ at 3582 cm^{-1}, $La(OH)_3$ at 3600 cm^{-1} and $Mg(OH)_2$ at 3650 cm^{-1} are displayed in Fig. 3a. Difference in wavenumber is large enough to distinguish between the different hydroxides. Raman spectra of La_2Ni_7 soaked 48 h and 12 weeks are given in Fig. 3b. For 48 h the corrosion layer is formed of $Ni(OH)_2$ or $La(OH)_3$, pure phases but not spatially homogeneous. For 12 weeks the corrosion layer is homogeneous and formed of a mixture of pure phases of $Ni(OH)_2$ and $La(OH)_3$.

In the presence of magnesium in the alloy, the Raman spectra are given in Fig. 3c for 8 weeks into KOH. The corrosion layer is spatially heterogeneous at the micrometre scale. A new band is appearing at 3650 cm^{-1} and attributed to $Mg(OH)_2$. The band corresponding to $Ni(OH)_2$ is shifted at 3590 cm^{-1} and in some spectra an enlargement of the high wavenumber side of the band corresponding to $La(OH)_3$ is visible.

The low frequency spectra (see supplementary information Fig. S4) recorded for the 12-weeks corroded sample indicate also the presence of $Mg(OH)_2$, but a very broad band around 540 cm^{-1} is also present, which could be attributed to a NiO or MgO oxide phase.

3.3. Morphologic and elemental characterisations of corrosion products

The first morphologic characterisation of corrosion products was performed with systematic SEM analysis for each corrosion

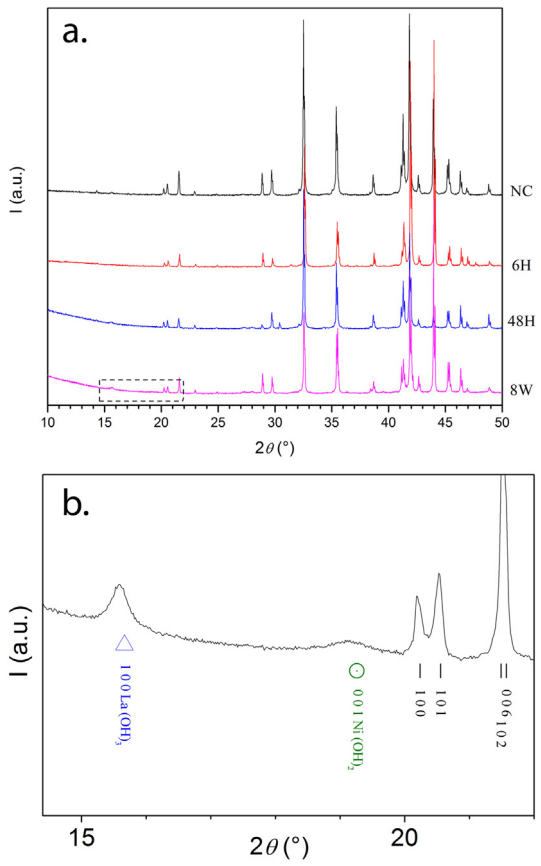

Fig. 1. La_2Ni_7 diffractograms after various immersion times in 8.7 M KOH; a. from top to bottom: non corroded (NC), 6 h (6H), 48 h (48H) and 8 weeks (8W); b. low theta region shown in the dashed rectangle, with longer acquisition time for the sample soaked 8 weeks in 8.7 M KOH. The (100) diffraction peak of $La(OH)_3$ (triangle; PDF n°00-036-1481) and the (001) diffraction peak of $Ni(OH)_2$ (circle; PDF n°04-012-5845) are shown beside the peaks of the main phase (vertical bars; Ce_2Ni_7-type).

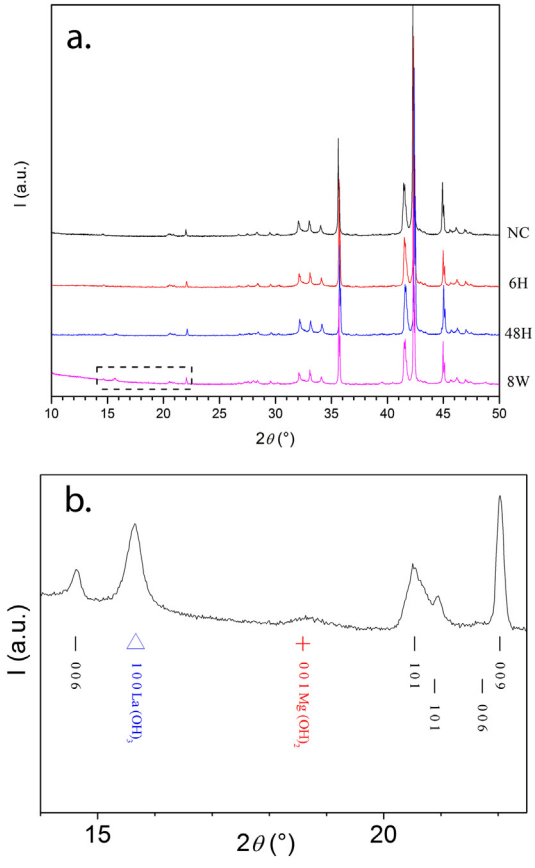

Fig. 2. $La_{1.5}Mg_{0.5}Ni_7$ diffractograms after various immersion times in 8.7 M KOH; a. from top to bottom: non corroded (NC), 6 h (6H), 48 h (48H) and 8 weeks (8W); b. low theta region shown in the dashed rectangle, with longer acquisition time for the sample soaked 8 weeks in 8.7 M KOH. The (100) diffraction peak of $La(OH)_3$ (triangle; PDF n°00-036-1481) and the (001) diffraction peak of $Mg(OH)_2$ (cross; PDF n° 00-007-0239) are shown beside the peaks of the main phases (vertical bars; Ce_2Ni_7- and Gd_2Co_7-type respectively).

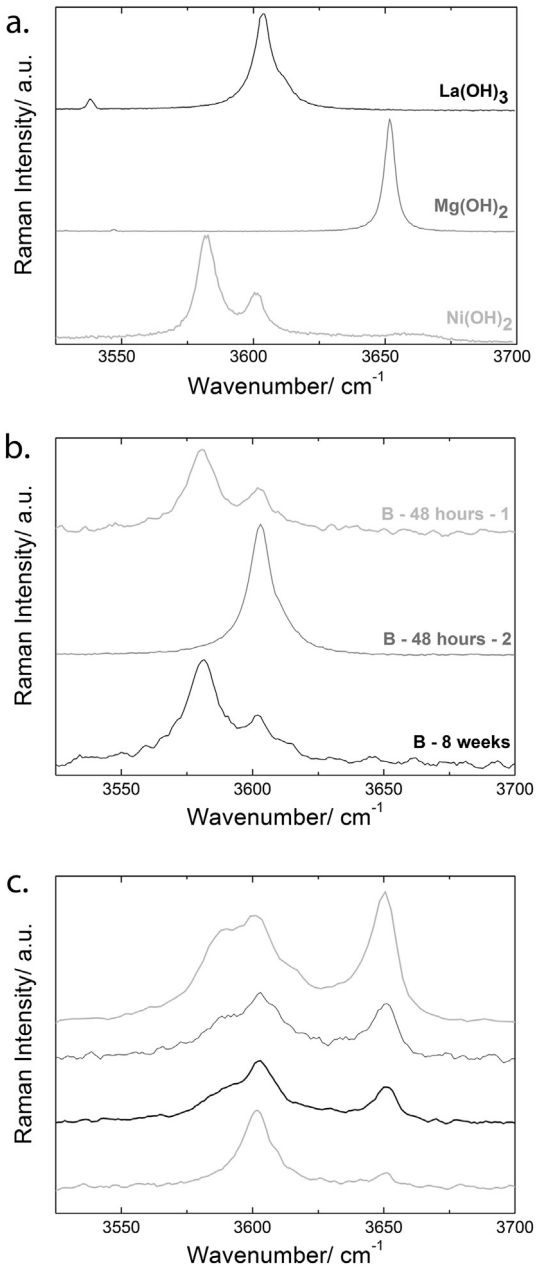

Fig. 3. Micro-RS spectra recorded on a. $La(OH)_3$, $Ni(OH)_2$ and $Mg(OH)_2$ references; b. La_2Ni_7 corroded for 48 h (2 points) and 8 weeks; c. $La_{1.5}Mg_{0.5}Ni_7$ corroded for 48 h (4 points). Acquisition conditions 600 s.

time. Some of the results are presented here for La_2Ni_7 and $La_{1.5}Mg_{0.5}Ni_7$ (Fig. 4) for low magnification in SE2 mode (additional micrographs are available in the Supplementary Information Figs. S2 and S3). The La_2Ni_7 surface is covered after 48 h of immersion in 8.7 M KOH. The $La_{1.5}Mg_{0.5}Ni_7$ surface is covered after 4 days of immersion in 8.7 M KOH. The corrosion product quantity seems quite the same for both alloys and do not vary whatever the immersion time over a few days.

Higher magnification micrographs in InLens mode (Fig. 5) present the morphology of the corrosion products developed on both alloys.

Needle-like morphology corrosion products appear first for the La_2Ni_7 alloy. Then hexagonal platelets appear. For the $La_{1.5}Mg_{0.5}Ni_7$ alloy, both platelets and needles appear for 6 h immersion in 8.7 M KOH.

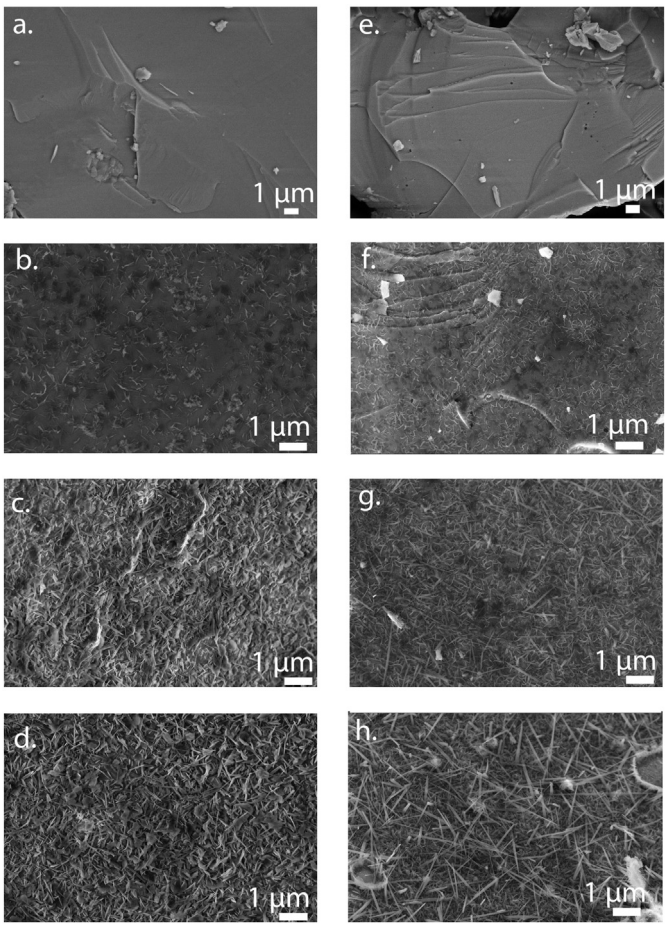

Fig. 4. SEM micrographs at magnification 10k, in SE2 mode, of (a.) non corroded La_2Ni_7 sample and La_2Ni_7 sample corroded for (b.) 6 h, (c.) 48 h and (d.) 8 weeks; (e.) non corroded $La_{1.5}Mg_{0.5}Ni_7$ sample and $La_{1.5}Mg_{0.5}Ni_7$ sample corroded for (f.) 6 h, (g.) 48 h and (h.) 8 weeks.

After 48 h immersion two morphologies are confirmed for both alloys. The first one corresponds to little platelets without size growth. The second one develops needle-like morphology. It is particularly evidenced for the pseudo-binary alloy. In this case, the needles are quite large, up to a micronic size, and they have a well defined morphology. For the binary alloy, the needles are smaller and less defined.

Fig. 6 presents SEM micrographs of both samples, focussing on the interface between the alloy and the corrosion products. This interface, which is smooth for the non-corroded alloys, shows a nanometric roughness as soon as the corrosion process starts.

Characterisation was completed by TEM analysis for the 48 h corroded samples. Fig. 7 presents elemental mapping for the 48 h corroded binary sample. The selected area shows two types of corrosion products. The one from the bottom, as can be seen in the TEM-mode micrograph, has a well-defined morphology with linear border despite its small size. This particle is associated with the La element. The corrosion particle in the upper part of the mapping is not so well defined, and is associated to the Ni element. La and Ni are segregated in the corrosion products, they form $La(OH)_3$ and $Ni(OH)_2$ hydroxides at different places and not in a single compound, as confirmed by electronic diffraction (see supplementary information Fig. S5 and Table S1).

Fig. 8 displays the elemental mapping for the 48 h corroded pseudo-binary sample. Well defined particles with needle-shape morphology can be distinguished. They are outstandingly linked

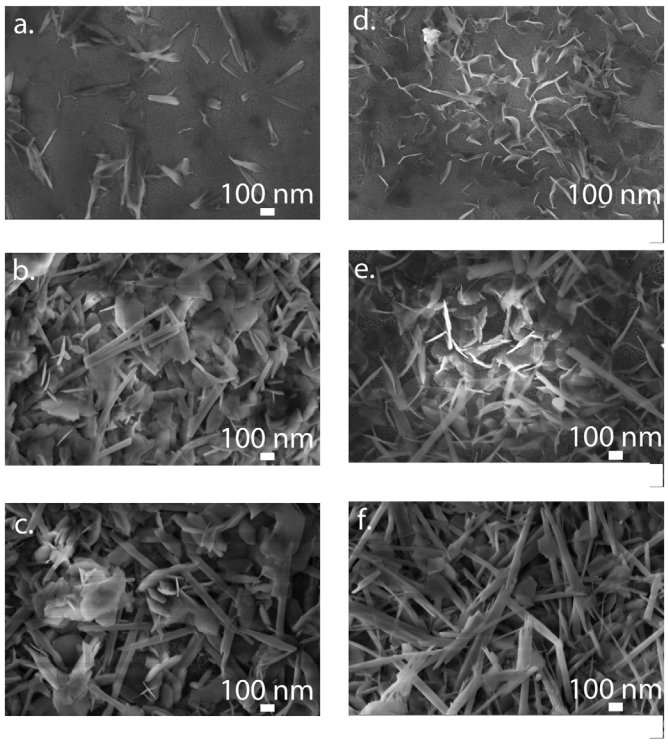

Fig. 5. SEM micrographs at magnification 50k, in InLens mode, of La_2Ni_7 sample corroded for (a.) 6 h, (b.) 48 h and (c.) 8 weeks on the left and $La_{1.5}Mg_{0.5}Ni_7$ sample corroded for (d) 6 h, (e.) 48 h and (f) 8 weeks on the right.

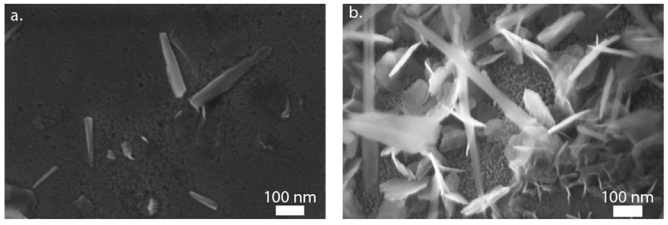

Fig. 6. SEM micrographs, in InLens mode, of the metal/corrosion products interface for a.La_2Ni_7 corroded for 6 h in 8.7 M KOH and b. $La_{1.5}Mg_{0.5}Ni_7$ corroded for 24 h in 8.7 M KOH.

to the La element in the STEM-EDS elemental mapping. Beside these needles, the other corrosion products are very fine. They are associated to the Mg element, as well as the Ni one.

Electronic diffraction allows to assign $La(OH)_3$ as the well-defined large needles. For the Ni and Mg containing area, no single crystallized area was found to allow measuring diffraction angles and interplanar distances with enough accuracy to differentiate between $Ni(OH)_2$ and $Mg(OH)_2$ hydroxides (see supplementary information Fig. S6 and Table S2).

Other TEM micrograph for binary and pseudo-binary samples corroded 6 h, 48 h and 8 weeks confirm the presence of two morphologies for both alloys: large and well defined needles for $La(OH)_3$ and small platelets of $Ni(OH)_2$ for La_2Ni_7 and of $Ni(OH)_2$/$Mg(OH)_2$ or (Mg, Ni)$(OH)_2$ particles for $La_{1.5}Mg_{0.5}Ni_7$.

Moreover, an inner channel can be observed inside the core of the $La(OH)_3$ needles. Fig. 9 presents the EDS profile of a $La(OH)_3$ needle for the pseudo-binary sample corroded 6 h. The profile is recorded along the transversal part of the needle. A La and O depletion appears in the middle of the needle. This indicates the presence of a hollow channel with a diameter about 2 nm.

Fig. 10 presents the micrographs for the 8-weeks pseudo-binary corroded sample. The large needles show a density variation in their central part. At the bottom of Fig. 10a, a hexagonal particle is observed with a small hole in its central part. EDS analysis indicates that these hexagonal particles are composed of La and O, identifying them as the $La(OH)_3$ needles in a transversal view. The diameter of the hole is about 10 nm diameter though this value should be taken with caution as part of the hole can be covered during the ultra-microtome preparation. It indicates however that the size of the hole might vary depending of the immersion time.

3.4. Specific corrosion of magnesium

Beside the general corrosion process detailed in this paper, small cubic particles have been also observed by SEM (Fig. 11a). The particle size is about 2 μm. EDS spectra performed on these particles indicate the presence of O and Mg (Fig. 11b). These elements, combined with the morphology observation, indicate that MgO crystals are present in the initial pseudo-binary alloy. These MgO crystals are attributed to Mg corrosion taking place at high temperature during the elaboration process. They disappear after two weeks in 8.7 M KOH. As suggested by the SEM micrograph (Fig. 11c) they probably turn into $Mg(OH)_2$ hexagonal platelets, thermodynamically favoured at such basic pH. These MgO particles are not identified in the XRD analysis, due to their very low concentration in the sample, and the low diffraction structure factors of Mg and O.

4. Discussion

4.1. Corrosion mechanisms in binary alloy

The corrosion process identified for La_2Ni_7 immersed in 8.7 M KOH can be described as a multilayer system with the following sequences: the metallic alloy/a rough alloy-corrosion products interface/corrosion products with large needles of $La(OH)_3$ and little platelets of $Ni(OH)_2$. The morphology of these platelets and needles are in good agreement with the crystallographic structures of these two phases.

The various immersion times evidence that the metallic grains are totally covered with hydroxides in 2 days. After 4 days of immersion, the platelets are well organised and no size growth can be noticed up to 16 weeks of exposure.

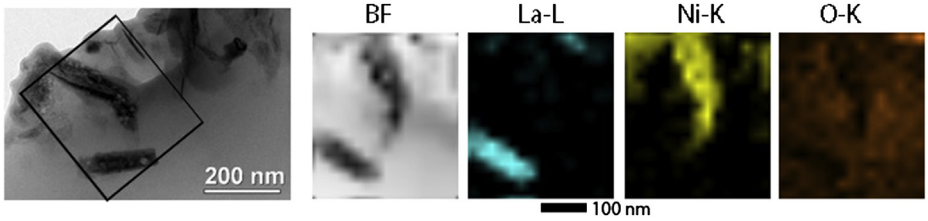

Fig. 7. TEM micrograph and EDS-STEM elemental mapping of La, Ni and O for the La_2Ni_7 sample corroded 48 h in 8.7 M KOH solution.

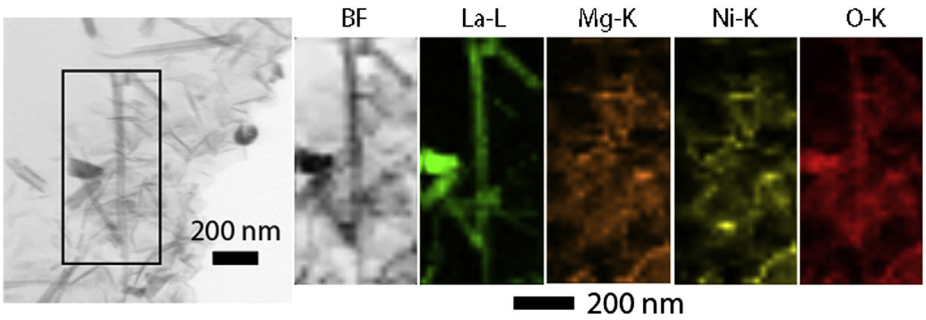

Fig. 8. TEM micrograph and EDS-STEM elemental mapping of La, Mg, Ni and O on $La_2Mg_{0.5}Ni_7$ sample corroded 48 h in 8.7 M KOH.

Unlike Maurel et al. [6], we evidenced the presence of $Ni(OH)_2$ that they did not point out. That could be explained by the low diffraction power of nickel hydroxide, and by the absence of Raman spectroscopy in their study. The rough interface layer formation can be explained by the internal oxidation mechanism. This layer is commonly associated to a metallic nickel amorphous layer which catalyses the surface electrochemical reaction, as suggested in Ref. [6] (Fig. 12).

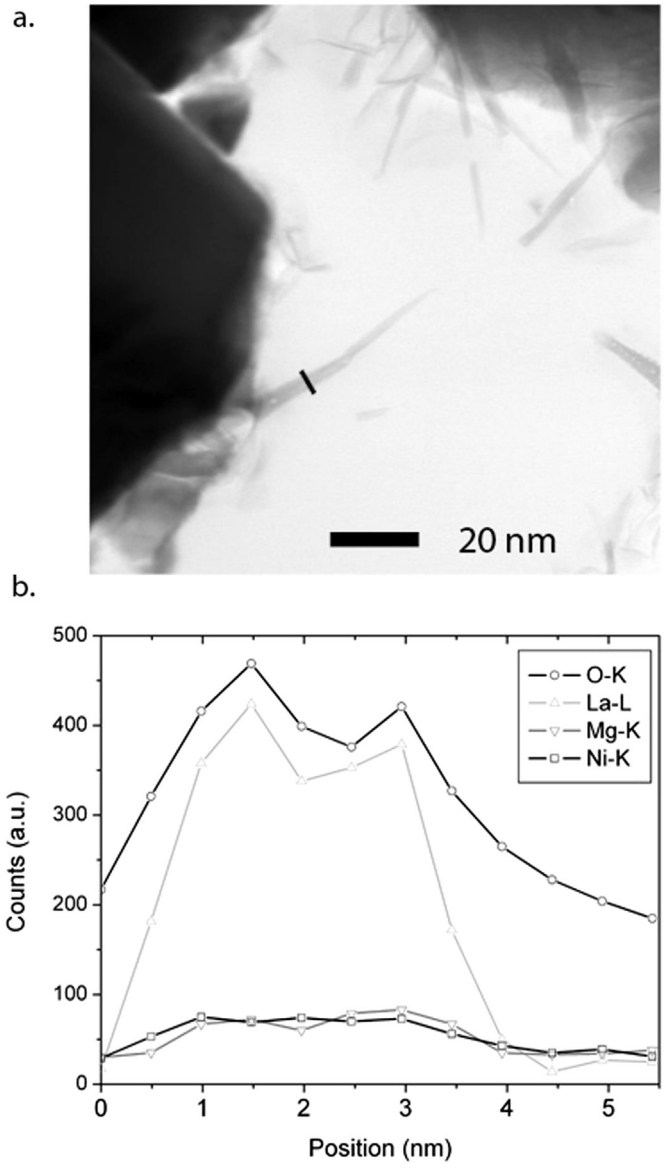

Fig. 9. STEM micrograph and STEM-EDS elemental profile for the $La_2Mg_{0.5}Ni_7$ sample corroded 6 h in 8.7 M KOH.

4.2. Influence of Mg on the corrosion mechanism

Considering the $La_{1.5}Mg_{0.5}Ni_7$ ternary alloy, the corrosion mechanism is strongly influenced by the presence of Mg. First, $Ni(OH)_2$ is no more observed as a pure phase in the XRD diagrams, and $Mg(OH)_2$ is detected. Therefore, it seems that the $Mg(OH)_2$ formation predominates as Mg is introduced in the alloy.

The micro-RS low frequency spectra recorded for the 12-weeks corroded sample indicates also the presence of $Mg(OH)_2$, as well as a very broad band around 540 cm^{-1}, which could be attributed to an oxide. Neither NiO nor MgO structures display a Raman signal as they have both face centered cubic structure. However, these crystals frequently include some impurities, or are non-stoichiometric with $Ni_{1-x}O$ or $Mg_{1-x}O$ formulae. In these cases, a broad band around 540 cm^{-1} appears. The presence of NiO or MgO oxides in our system could result from the dehydration of the hydroxide phases, leading to oxide formation. This dehydration is likely to appear under the Raman laser beam.

Considering the STEM-EDX elemental mapping of the pseudo-binary sample, two morphologies are identified: large needles composed of La and O, corresponding to the $La(OH)_3$ phase, and small particles. These are linked to the Mg element, as could be deduced from the XRD $Mg(OH)_2$ identification, but they are also related to the Ni element. Therefore two hypotheses are proposed for this observation. $Mg(OH)_2$ and $Ni(OH)_2$ hydroxides can both be present, finely mixed at the nanometric scale, or Mg can substitute Ni in the $Mg(OH)_2$ hydroxide, the only one identified by XRD analyses.

To choose between these two hypotheses, the cell parameters have been derived from the X-ray diffractogram shown in the inset of Fig. 2. They are presented in Table 2. The cell parameters for $Mg(OH)_2$, as identified in the corroded pseudo-binary alloy, have intermediate values between those of pure $Mg(OH)_2$ and pure

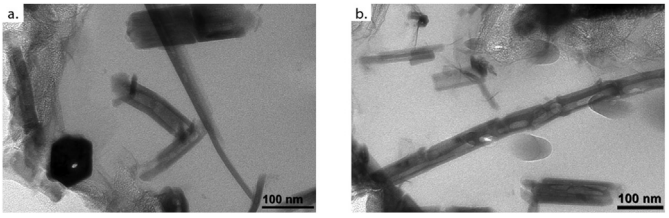

Fig. 10. TEM micrographs showing the tubular structure on $La_2Mg_{0.5}Ni_7$ sample corroded 8 weeks in 8.7 M KOH.

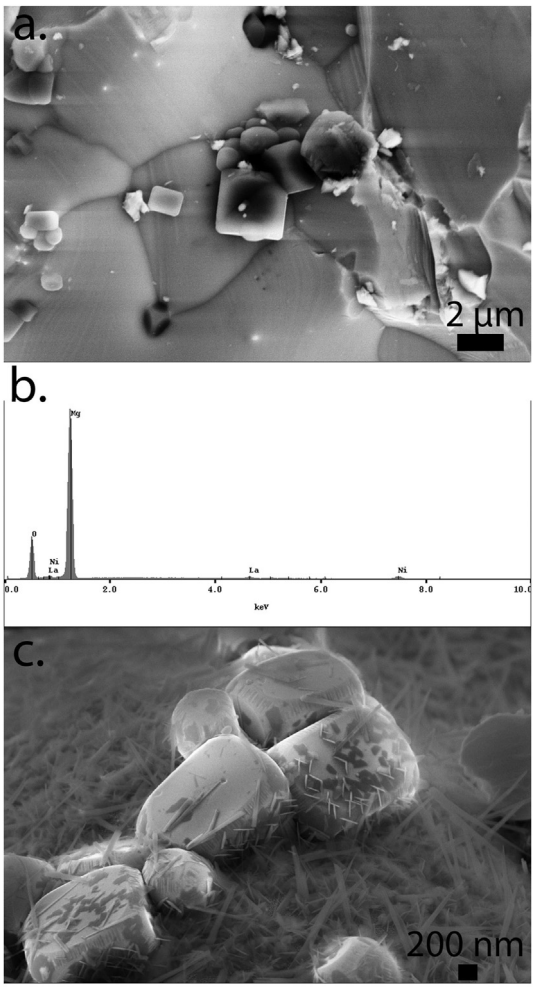

Fig. 11. a. SEM micrograph and b. SEM-EDS analysis on $La_2Mg_{0.5}Ni_7$ sample non-corroded, focussing on cubic crystal of MgO. c. SEM micrograph showing MgO crystals being transformed into $Mg(OH)_2$ in the $La_2Mg_{0.5}Ni_7$ sample corroded 48 h in 8.7 M KOH.

$Ni(OH)_2$. The *a* parameters are very close for both phases, however the *c* parameters are significantly different. In the refined pattern, the main diffraction peak for $Mg(OH)_2$ is the (001) one, giving a value of the *c* parameter for the 8-weeks corroded pseudo-binary sample in between those of $Mg(OH)_2$ and $Ni(OH)_2$ favouring the second hypothesis. Considering the weak diffraction factor of Mg, and the low $Mg(OH)_2$ content in the sample, this result has to be considered with cautious but suggests that Ni is substituted within the $Mg(OH)_2$ lattice.

Table 2
Cell parameters for $La_{1.5}Mg_{0.5}Ni_7$ corroded 8 weeks in 8.7 M KOH compared to those of pure $Mg(OH)_2$ and $Ni(OH)_2$.

	$Mg(OH)_2$ (ref JACGAR 1996 29 48-52)	$La_{1.5}Mg_{0.5}Ni_7$ corroded 8 weeks	$Ni(OH)_2$(ref JPSODZ 2007 174 414-420)
a	3.1477	3.1472	3.1260
c	4.7717	4.7345	4.6050

In the presence of magnesium, the Raman spectrum of lanthanum hydroxide is not modified but $Mg(OH)_2$ as pure phase is identified by the band at 3650 cm^{-1}. The O–H vibration of $Ni(OH)_2$ is 10 cm^{-1} shifted showing that $Ni(OH)_2$ as pure phase is not formed anymore. Solid solution of Ni/Mg hydroxide has been studied by infrared spectroscopy and O–H vibration depends quite linearly on the Mg/Ni content of the solid solution [14]. The spatial variation of the recorded Raman spectra at the micrometre scale clearly indicates that the corrosion product layer is formed from: $La(OH)_3$ and $Ni_{1-x}Mg_x(OH)_2$ with x varying from one point to another. The formation of Ni/Mg hydroxide by coprecipitation technique has already been studied and different compositions can be formed depending on the process for the same solution content [15]. However the existence of a predominant defined composition in the corrosion layer cannot be excluded as Raman spectroscopy is not a quantitative technique.

These observations lead to the conclusion that in the La–Mg–Ni system, Mg and Ni are involved in the same hydroxide formation, with a $Mg(OH)_2$ structure including Ni in its lattice, forming a mixed (Mg, Ni)$(OH)_2$ hydroxide. Neither this hydroxide, nor the $Ni(OH)_2$ hydroxide formed for La_2Ni_7, could modify the electrochemical capacity of the negative electrode, considering their compositions is very close to that of the positive electrode (i.e. at much higher hydrogenation potential). Moreover, as observed for AB_5 alloys, neither the (Ni, Mg)$(OH)_2$ nor the $La(OH)_3$ needles affect the density of the catalytic metallic nickel layer.

Comparing the various immersion times, we evidence that the alloy surface is totally covered with hydroxides within 4 days as for the binary alloy it is covered within 2 days. The corrosion could start slower with the Mg. Moreover, the $La(OH)_3$ needles have a better defined morphology when Mg is present. This suggests that Mg promotes the ordering of the corrosion products. As concerns applications, the Mg rate in (R, Mg)Ni_x alloy has to be finely considered to reach the better compromise between the positive effect on plateau pressure and capacity and the effect related to corrosion of the alloy. Moreover, the presence of Mg in the alloy lead to specific oxidation mechanism of Mg, with the formation of MgO during the alloy elaboration. This corrosion product turns into $Mg(OH)_2$ with immersion non 8.7 M KOH.

Finally, the rare earth hydroxide needles show a channel in their central part. Maurel et al. showed that these channels play a role in

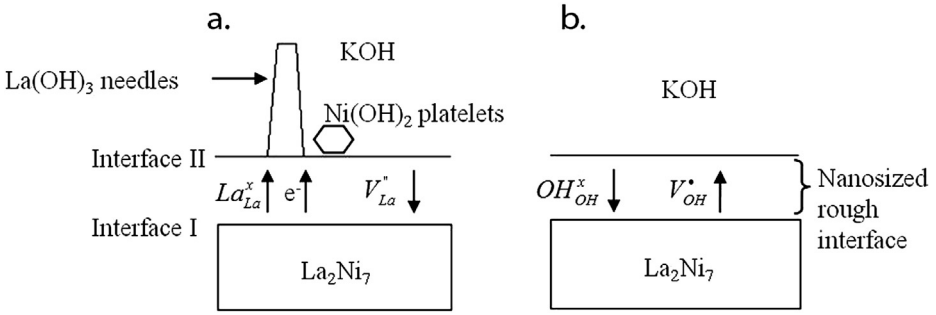

Fig. 12. Corrosion mechanisms by a. cationic and b. anionic transport as proposed by Maurel et al. [6], modified (this work) to introduce the presence of the $Ni(OH)_2$ platelets.

the growth mechanism [6]. These holes have nanometric dimensions, varying from 2 to 3 nm for the pseudo-binary sample corroded during 6 h up to 10 nm for the sample corroded 8 weeks. It is worth to note that those "nanochannels" have their diameter size growing with the needle size. This point is in contradiction with the previous work [6] on AB_5 sample for which they reported that the hole size staid constant for various immersion times.

5. Conclusion

The present study investigates two compounds: La_2Ni_7 and $La_{1.5}Mg_{0.5}Ni_7$ alloys and aims to understand from a fundamental point of view which corrosion products develop in A_2B_7 alloys when soaked in KOH. We focused our attention on the influence of Mg on corrosion mechanisms. It appears that A_2B_7 binary alloys corrode in the same way than AB_5 alloys, with formation of $Ni(OH)_2$ and $La(OH)_3$ hydroxides upon a rough interface. When magnesium is added, Mg hydroxide is observed instead of the Ni one. However Ni is probably substituted in the $Mg(OH)_2$ structure. The $La(OH)_3$ needles are better defined and longer than for the binary alloy. Moreover, specific corrosion due to the Mg has been observed. This modified corrosion of Mg-containing alloys requires establishing a compromise between the beneficial effect of Mg on the pressure plateau and capacity and its detrimental effect on the corrosion rate. In both alloys, the $La(OH)_3$ needles present inner nanochannels which play a role in the needle growth process.

Acknowledgements

P. Bernard and L. Goubault from SAFT-BATTERIES (Bordeaux, France), as well as V. Vivier from LISE, are gratefully acknowledged for useful discussions. The authors would like to thank V. Lalanne (ICMPE) for her help for TEM sample preparation and E. Leroy (ICMPE) for EPMA and TEM analyses.

The research program MALHYCE (ANR-2011-PRGE-006 01) is acknowledged for financial support.

Appendix A. Supplementary data

Supplementary data related to this article can be found at http://dx.doi.org/10.1016/j.jpowsour.2014.05.008.

References

[1] F. Lichtenberg, U. Köhler, A. Fölzer, N.J.E. Adkins, A. Züttel, J. Alloys Compd. 253–254 (1997) 570–573.
[2] Y. Liu, Y. Cao, L. Huang, M. Gao, H. Pan, J. Alloys Compd. 509 (2011) 675–686.
[3] A. Akiba, H. Hayakawa, T. Kohno, J. Alloys Compd. 408–412 (2006) 280–283.
[4] J. Chen, N. Kuriyama, H.T. Takeshita, H. Tanaka, T. Sakai, M. Haruta, Electrochem. Solid State Lett. 3 (2000) 249–252.
[5] T. Kohno, H. Yoshida, F. Kawashima, T. Inaba, I. Sakai, M. Yamamoto, M. Kanda, J. Alloys Compd. 311 (2000) L5–L7.
[6] F. Maurel, B. Knosp, M. Backhaus-Ricoult, J. Electrochem. Soc. 147 (2000) 78–86.
[7] M. Ikoma, K. Komori, S. Kaida, C. Iwakura, J. Alloys Compd. 284 (1999) 92–98.
[8] C. Khaldi, S. Boussami, B.B. Rejeb, H. Mathlouthi, J. Lamloumi, Mater. Sci. Eng. B Solid 175 (2010) 22–28.
[9] P. Leblanc, C. Jordy, B. Knosp, P. Blanchard, J. Electrochem. Soc. 145 (1998) 860–863.
[10] B. Liao, Y.Q. Lei, L.X. Chen, G.L. Lu, H.G. Pan, Q.D. Wang, J. Power Sources 129 (2004) 258–267.
[11] Y. Liu, H. Pan, M. Gao, Y. Lei, Q. Wang, J. Electrochem. Soc. 152 (2005) A1089–A1095.
[12] Y. Liu, H. Pan, M. Gao, Q. Wang, J. Mater. Chem. 21 (2011) 4743–4755.
[13] R.J. Gilliam, J.W. Graydon, D.W. Kirk, S.J. Thorpe, Int. J. Hydrogen Energy 32 (2007) 359–364.
[14] E.F. de Oliveira, Y. Hase, Vib. Spectrosc. 31 (2003) 19–24.
[15] A. Packtese, C. Uppaladinni, Cryst. Res. Technol. 19 (1984) 33–41.